Additive manufacturing of titanium alloys

Contents

- ❑ Introduction
- ❑ Ti-6Al-4V
- ❑ Commercially pure titanium
- ❑ β titanium alloys

Introduction

Table 1.1: The nominal composition of the most commonly AMed titanium alloys. All compositions are in weight percent, and the Ti content is balanced.

Alloy	Category	Al	V	C	Fe	Nb	Zr	Sn	Mo	Ta
Ti-6Al-4V	α+β	6	4	<0.1	<0.3	-	-	-	-	-
Commercially pure Ti	α	-	-	<0.1	<0.25	-	-	-	-	-
Ti-24Nb-4Zr-8Sn	β	-	-	-	-	24	4	8	-	-
Ti-13Nb-13Zr	β	-	-	-	-	13	13	-	-	-
Ti-15Mo	β	-	-	-	-	-	-	-	15	-
Ti-45Nb	β	-	-	-	-	45	-	-	-	-
TNZT	β	-	-	-	-	35	7	-	-	5

Ti-6Al-4V

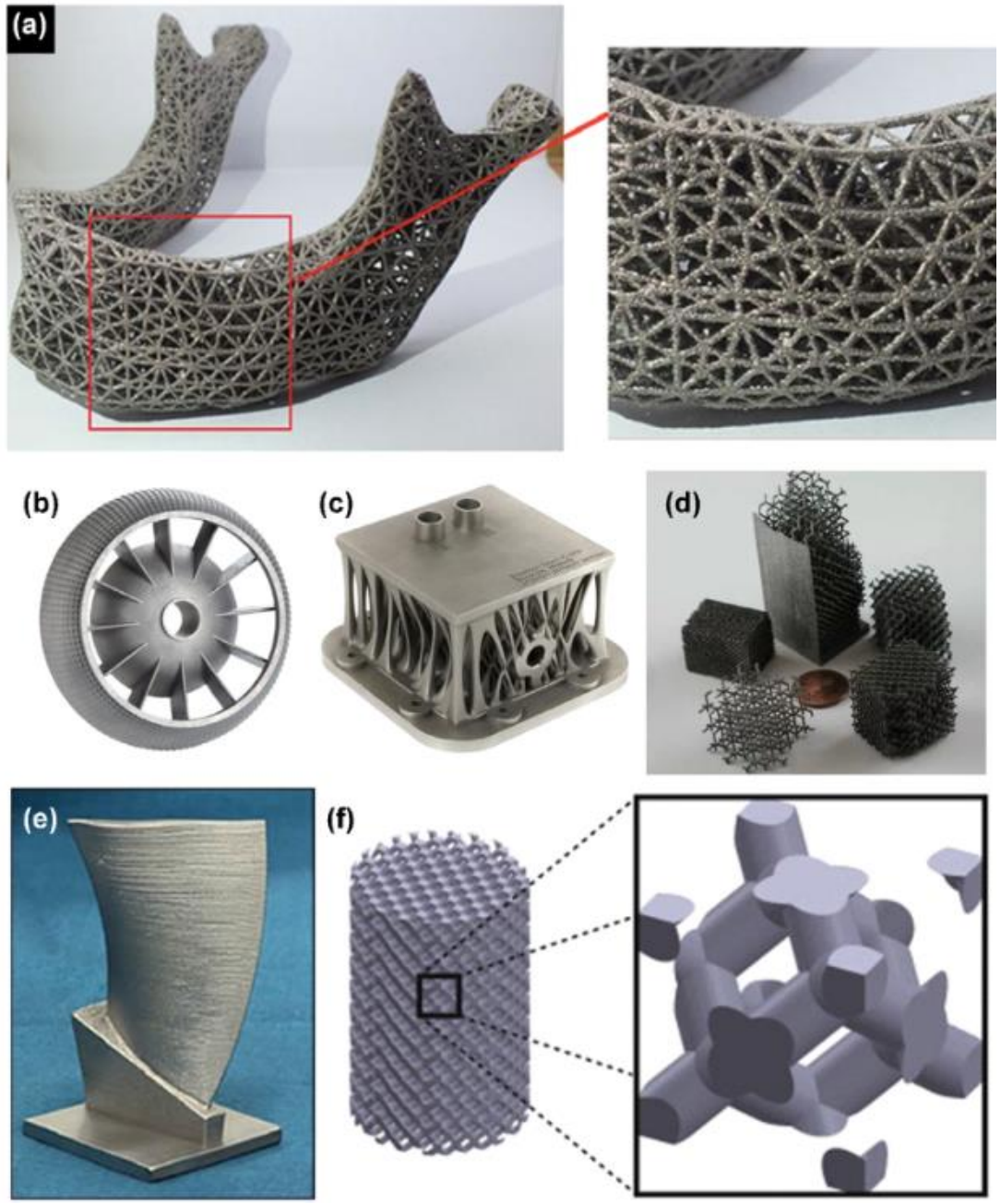

Fig. (a) EBM-fabricated 3D mesh Ti-6Al-4V mandibular prosthesis scaffold, (b) High precision Ti-6Al-4V air duct produced by LPBF without major rework, (c) EBMed Ti-6Al-4V medical components, (d) EBM-built lattice structured Ti-6Al-4V foams, (e) Ti-6Al-4V blade constructed with LMD, and (f) Ti-6Al-4V porous sample and LPBFed diamond unit cell

Source: Liu and Shin 2019 [https://doi.org/10.1016/j.matdes.2018.107552]

Ti-6Al-4V

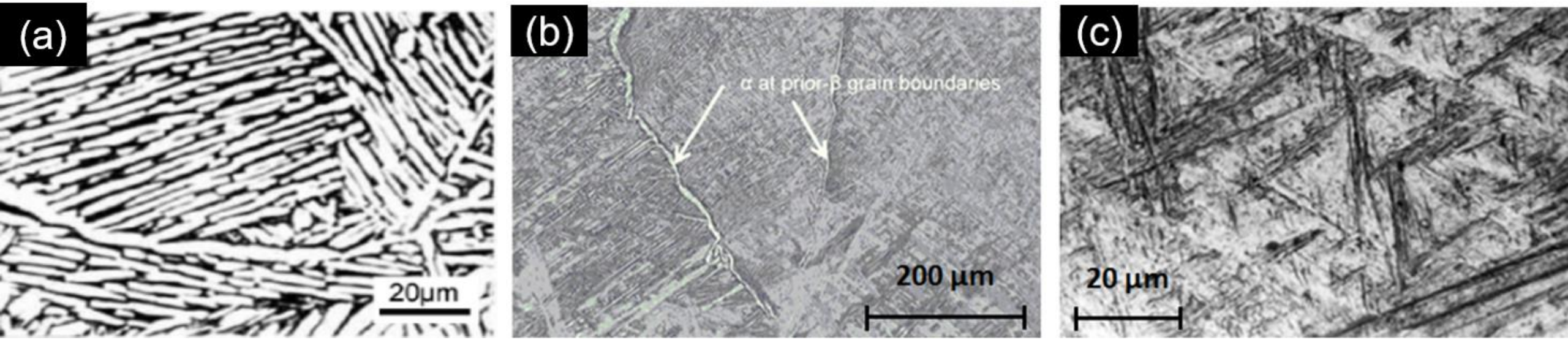

Microstructures of Ti-6Al-4V at room temperature. (a) Widmanstatten α with a intra-lamellar β phase (black phase), (b) grain boundary α, and (c) martensite (black laths in white β matrix)

Source: [a]Zhong et al. 2020 [https://doi.org/10.3390/app10030764]
[b], [c]Salsi et al. 2018 [https://doi.org/10.3390/met8080633]

Ti-6Al-4V

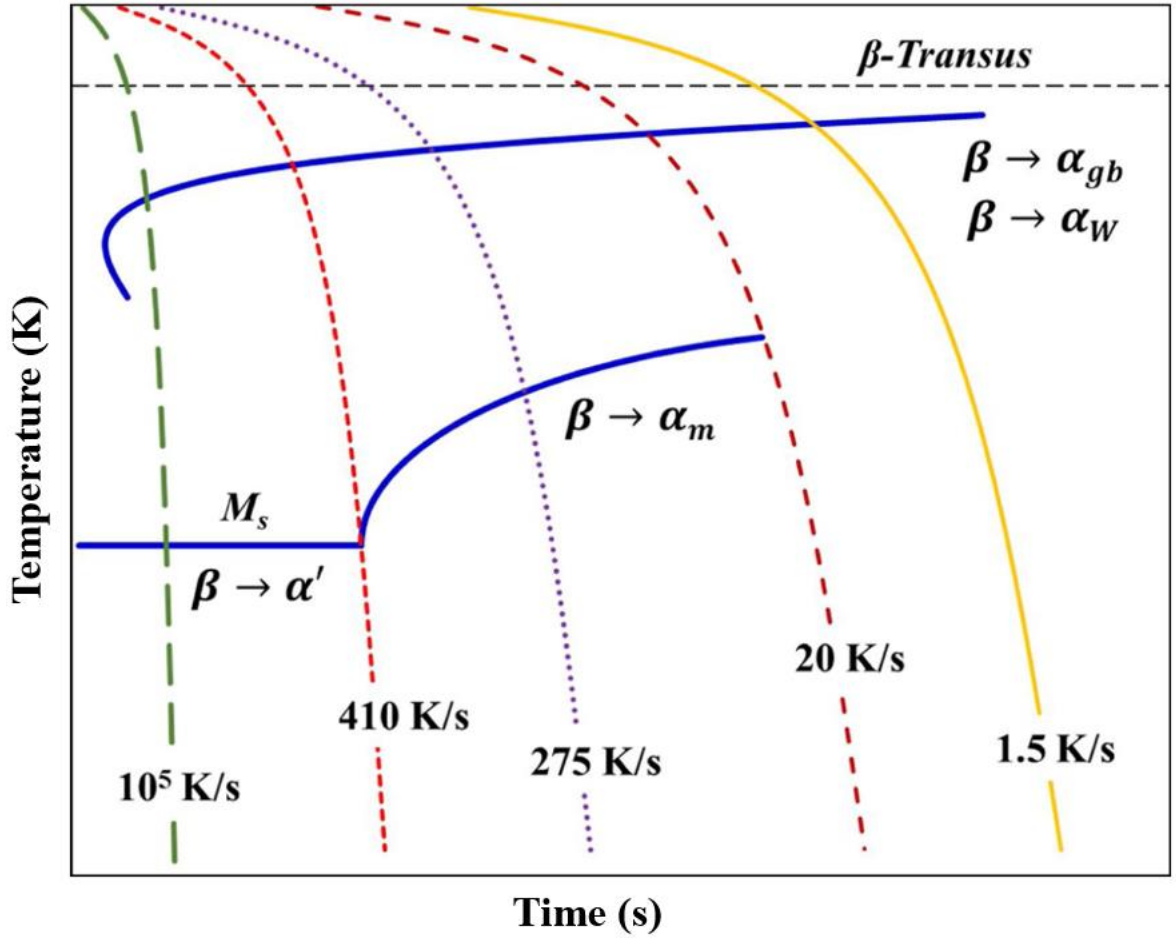

Fig. CCT diagram for Ti-6Al-4V with various cooling curves superimposed

Source: Wei et al. 2020 [https://doi.org/10.1016/j.addma.2020.101221]

Ti-6Al-4V

Ti-6Al-4V optical microstructures after various fabrication methods

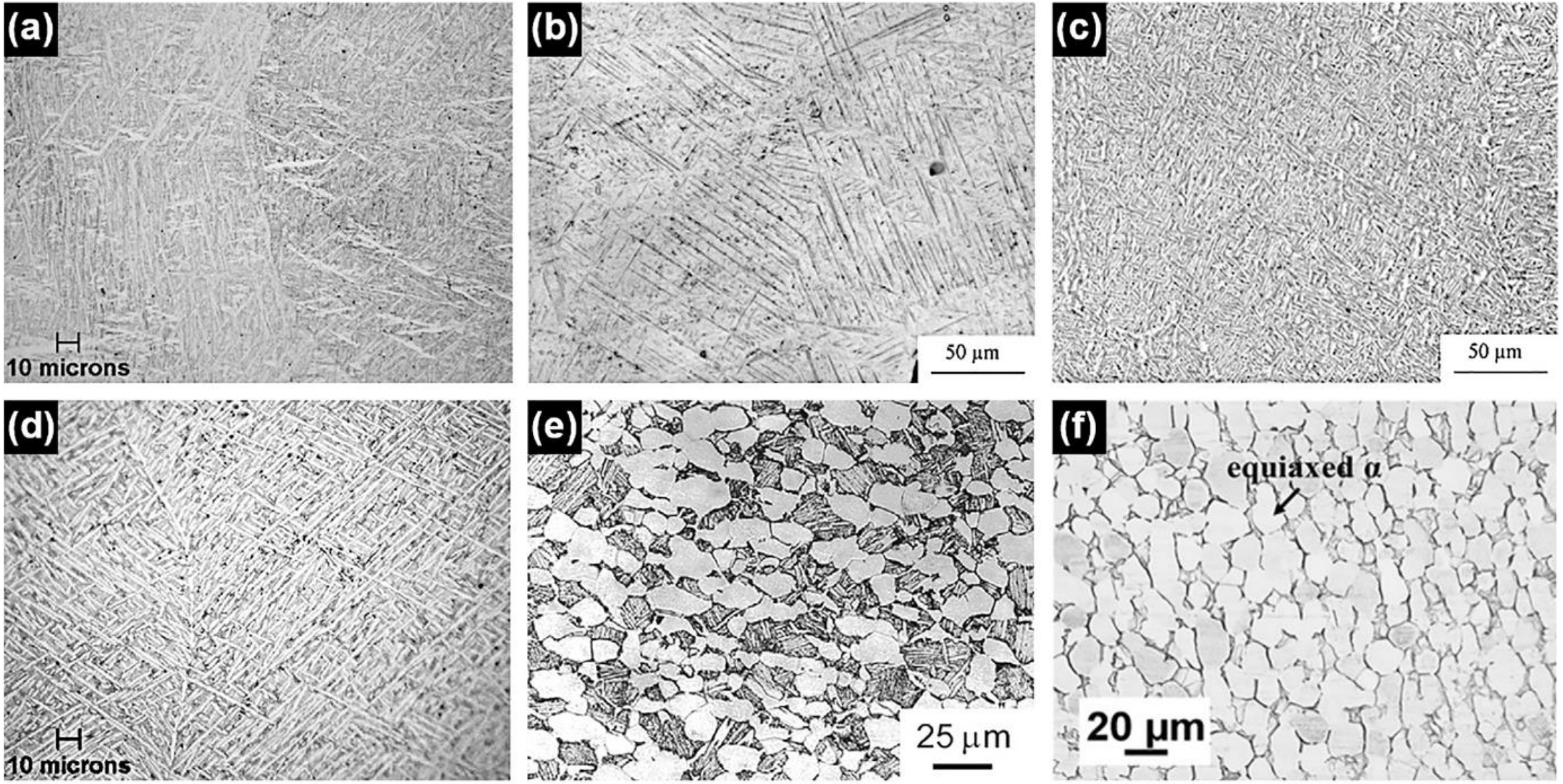

Fig. (a) LMDed Ti-6Al-4V yields an acicular α'-martensite phase, (b) LPBFed Ti-6Al-4V microstructures show α'-martensite (black laths) as well, (c) EBMed Ti-6Al-4V exhibits α (white)+β (black) dual phase, (d) An annealed microstructure of an LMDed Ti-6Al-4V shows α(white)+β (black) dual phase, (e) Solution treated and overaged wrought Ti-6Al-4V microstructure reveals equiaxed primary α (white) and secondary α+β lamellae (grains with crossings), and (f) Equiaxed α colony in mill-annealed Ti-6Al-4V

Source: Liu and Shin 2019 [https://doi.org/10.1016/j.matdes.2018.107552]

Ti-6Al-4V

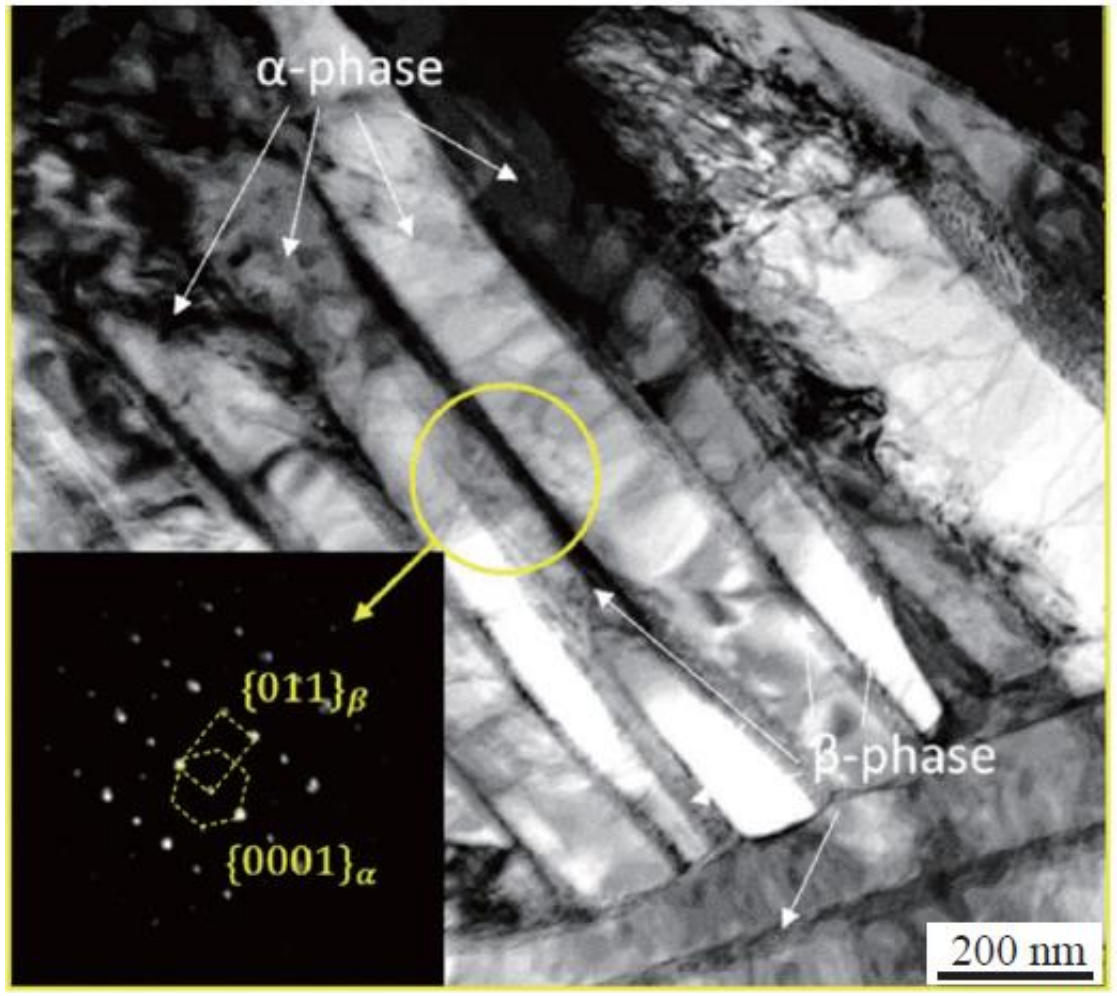

Fig. Representative TEM micrograph showing an α+β dual phase structure in LPBFed as-built Ti-6Al-4V

Source: Cao et al. 2021 [https://doi.org/10.37188/lam.2021.020]

Ti-6Al-4V

Fig. Three-track LMDed Ti-6Al-4V, the temporal and spatial temperature fields in the melt pool are generated at eleven different locations along the dashed line, where the extracted free surface (yellow line), melt pool (red line), and heat affected zone (green line) boundaries are superposed

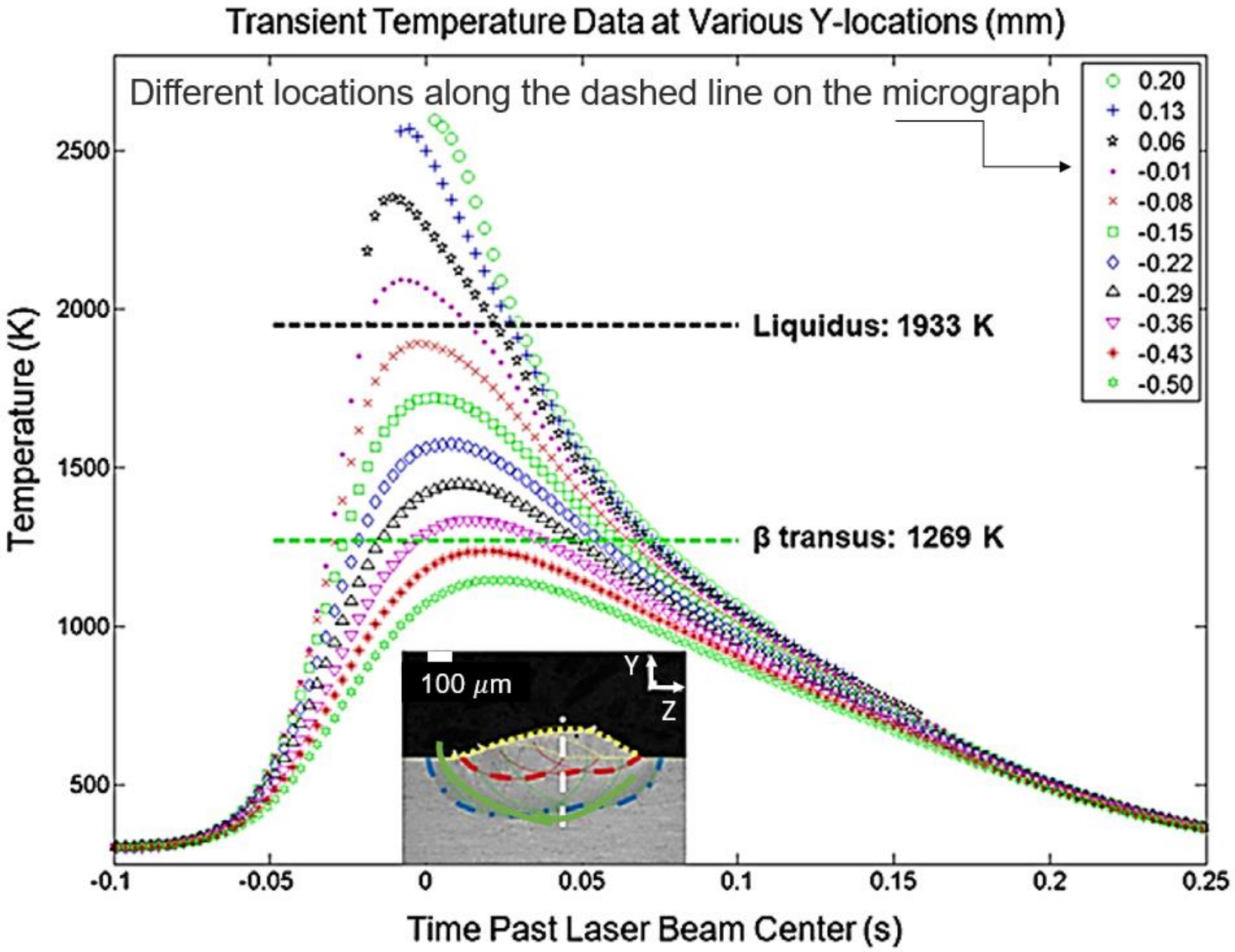

Source: Liu and Shin 2019 [https://doi.org/10.1016/j.matdes.2018.107552]

Ti-6Al-4V

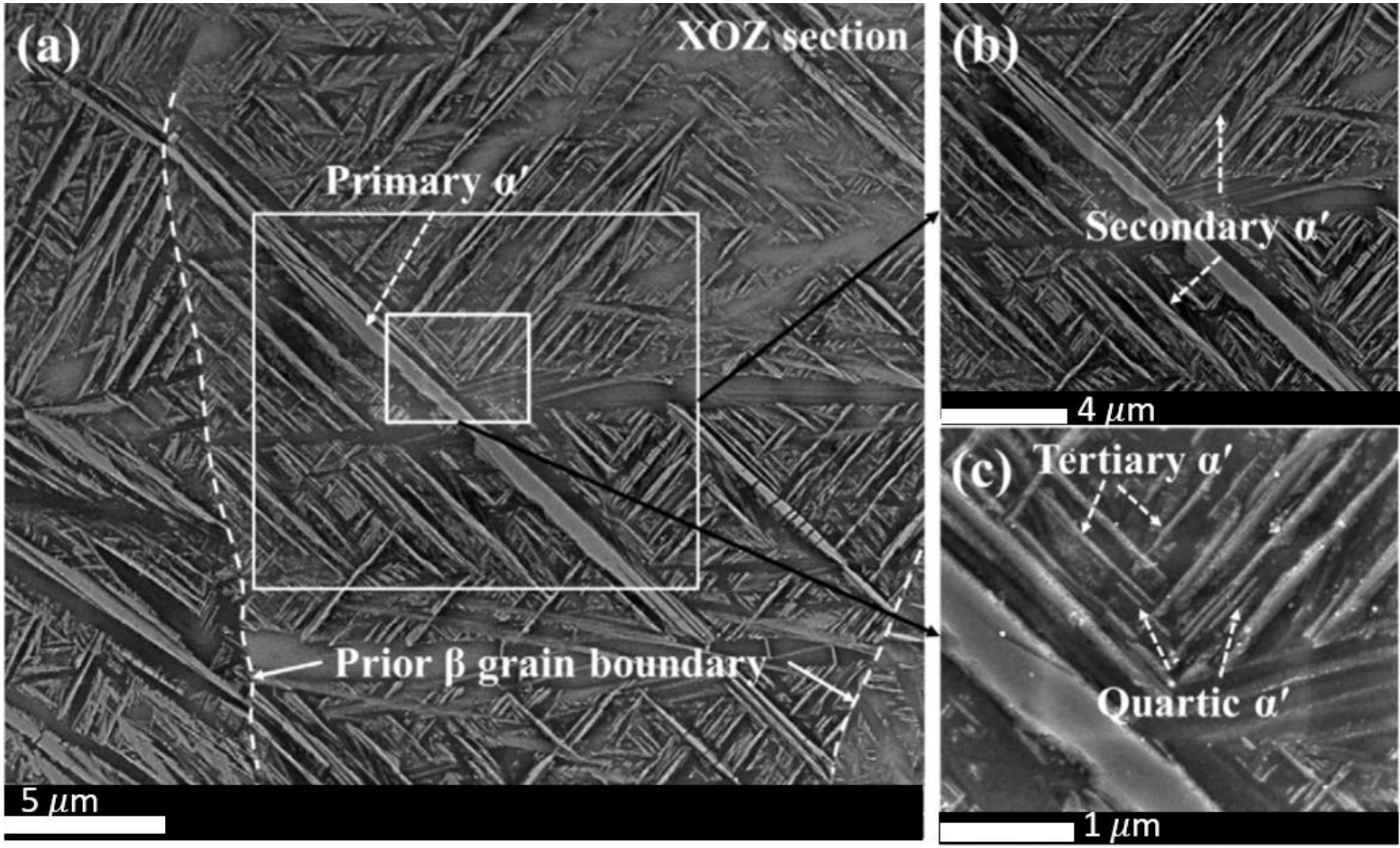

Fig. (a) SEM micrograph of an LPBFed Ti-6Al-4V on XOZ section (build direction), showing the hierarchy in martensite. (b) and (c) Magnified areas that are shown in rectangles in (a) to shown secondary, tertiary, and quartic martensite

Source: Yang et al. 2016 [https://doi.org/10.1016/j.matdes.2016.06.117]

Commercially pure titanium

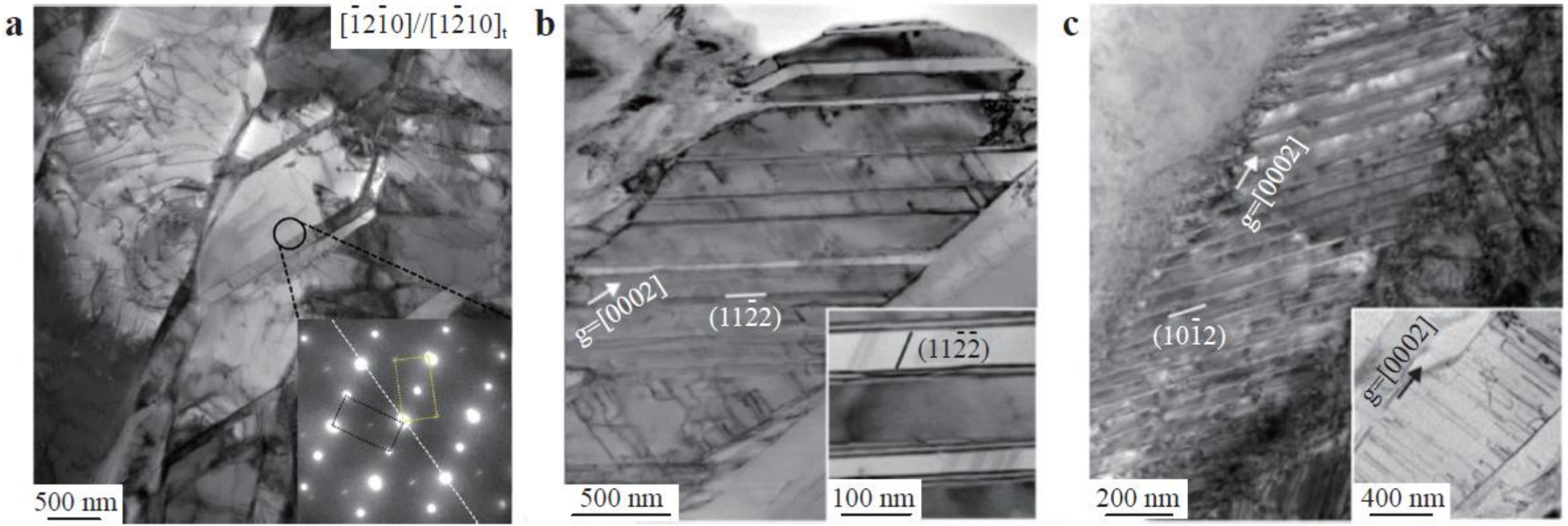

Fig. Twins and dislocations in LPBFed as-built Ti-6Al-4V. (a) Type l compression twin, (b) type ll compression twin, and (c) tension twin

Source: Cao et al. 2021 [https://doi.org/10.37188/lam.2021.020]

Commercially pure titanium

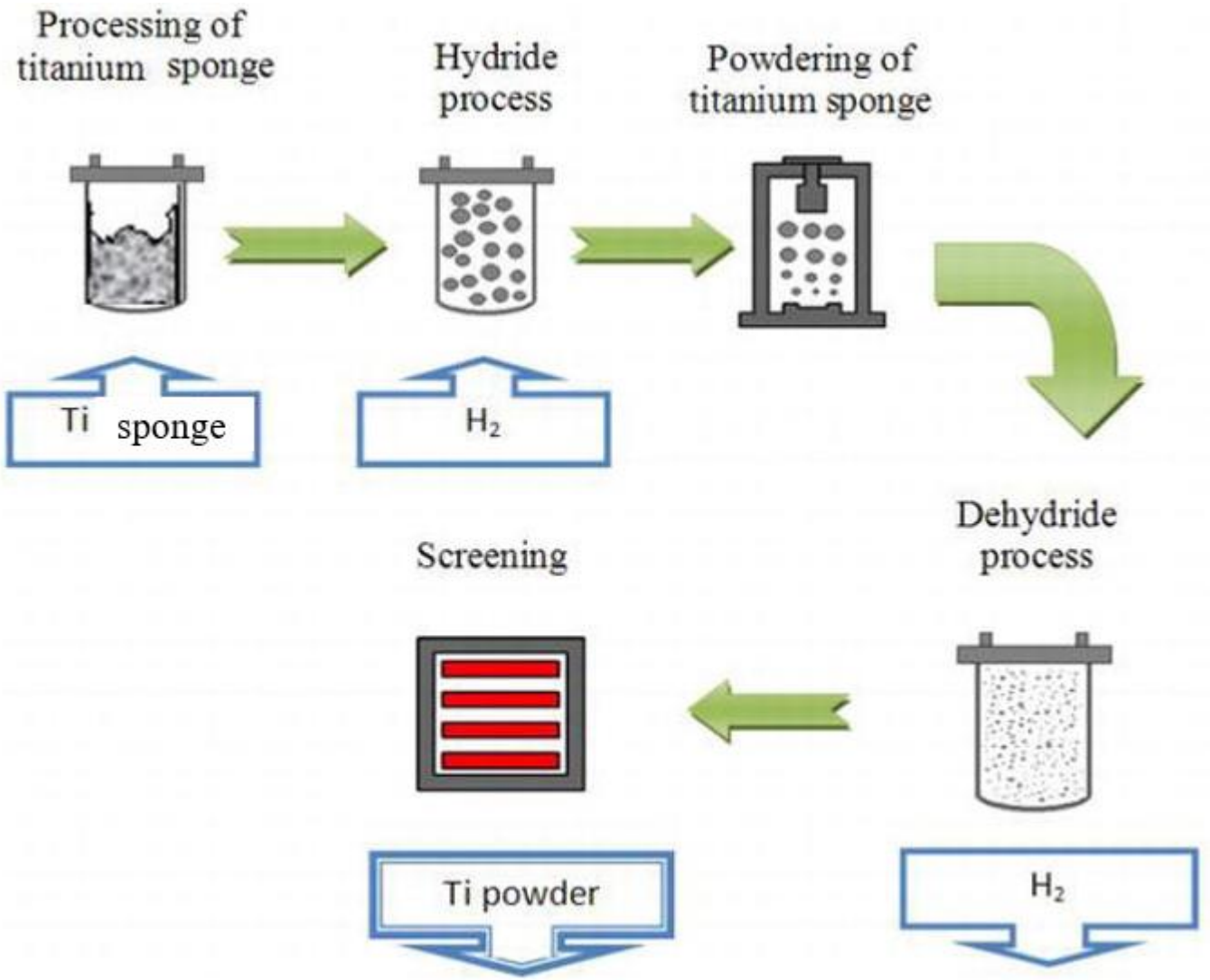

Fig. Schematics of hydride-dehydride process

Source: Ovchinnikov et al. 2016 [https://api.semanticscholar.org/CorpusID:208009098]

Commercially pure titanium

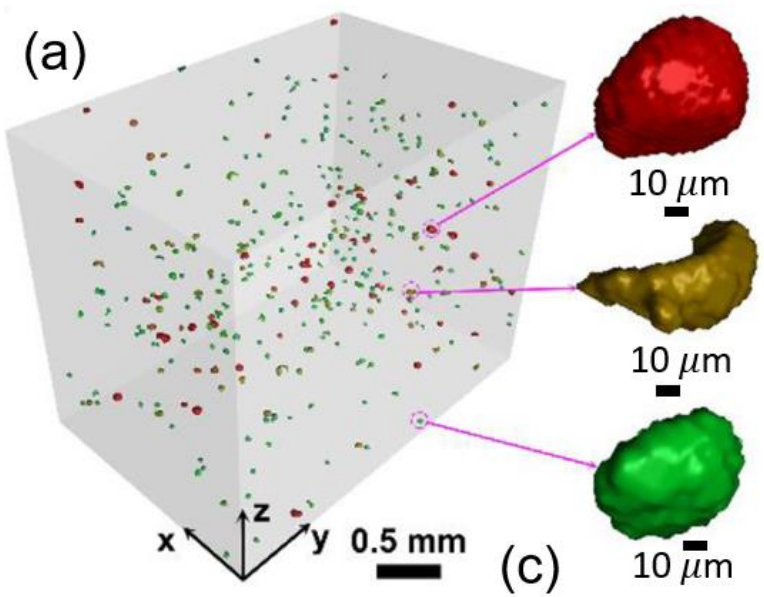

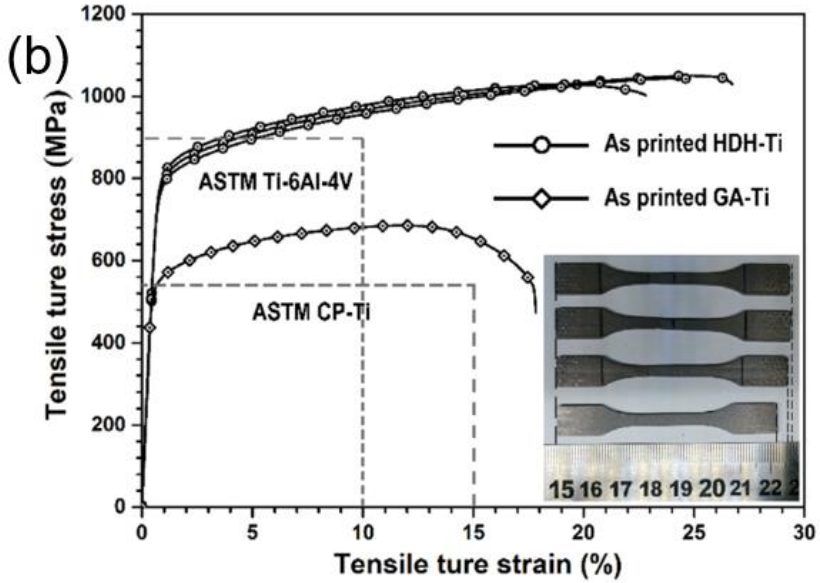

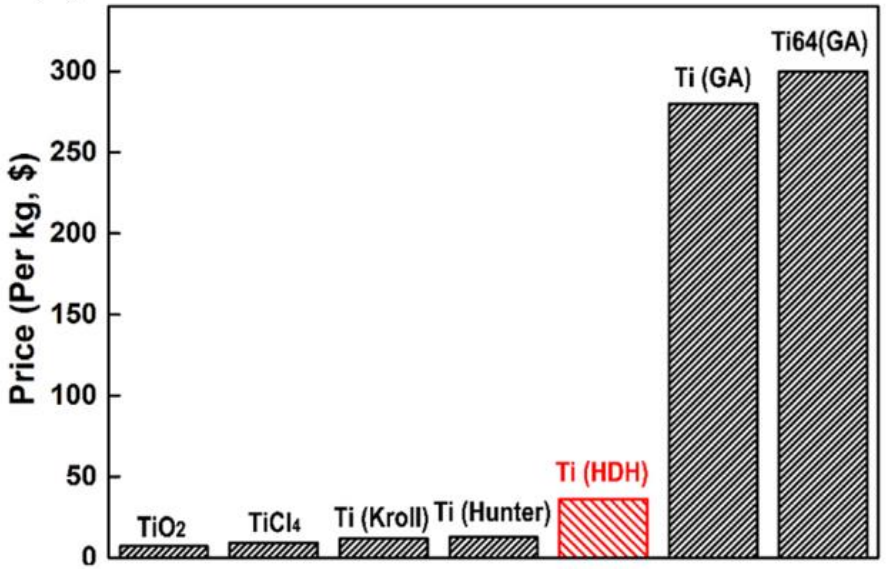

Fig. (a) A typical Micro-CT image of the LPBF as-built HDH-Ti sample with 3D reconstruction views. (b) Typical tensile true stress-strain curves of LPBF as-built HDH-Ti and GA-Ti samples, with an inset showing HDH-Ti samples before and after fracture. (c) Price comparison of titanium powders, including HDH-Ti powders, GA-Ti powder, and GA-Ti-6Al-4V powder

Source: Dong et al. 2020 [https://doi.org/10.1016/j.matdes.2020.109142]

Commercially pure titanium

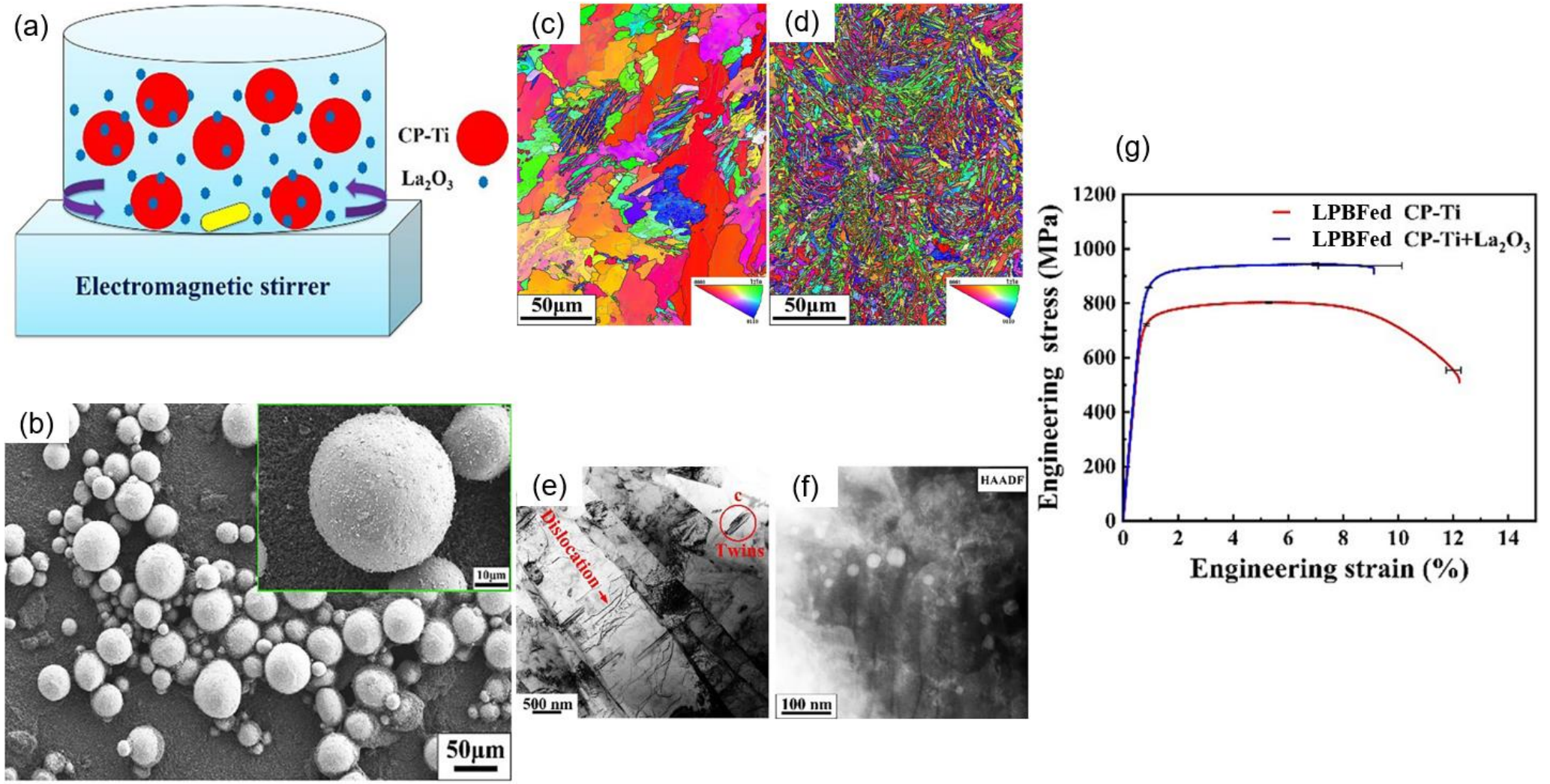

Fig. (a) Schematics of Electromagnetic stirring of composite powders, (b) Powder morphology images from SEM showing CP-Ti + La2O3 powder and typical surface (inset), (c) and (d) LPBF as-built CP-Ti and CP-Ti + La_2O_3, respectively, inverse pole figures measured in a section plane parallel to the building direction, (e) and (f) Bright field TEM images of the LPBF as-built CP-Ti and CP-Ti + La_2O_3, respectively. (g) Engineering stress-strain curves of LPBF as-built CP-Ti and CP-Ti + La_2O_3.

Source: Wang et al. 2021 [https://doi.org/10.1016/j.matchar.2021.111074]

Commercially pure titanium

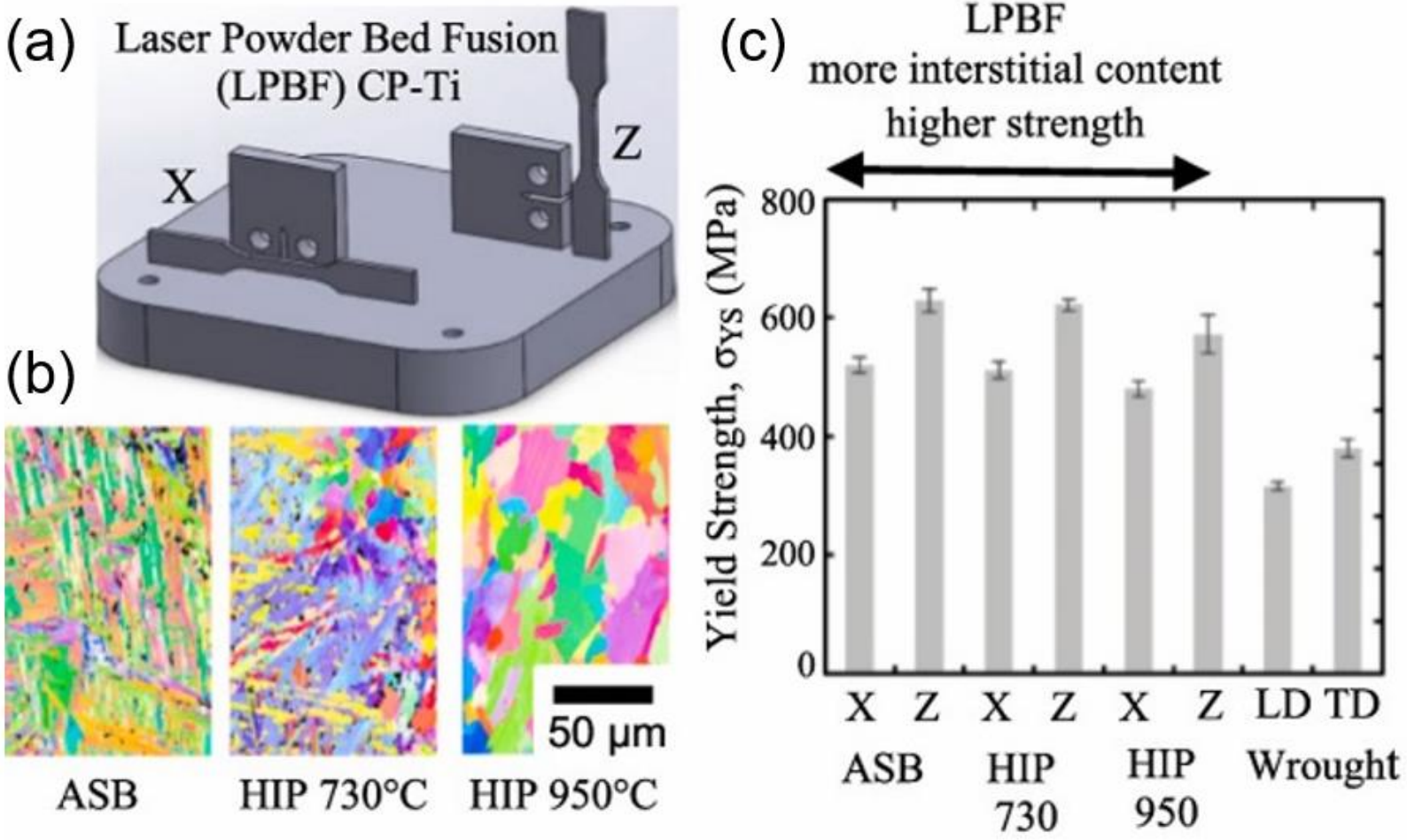

Fig. (a) Schematics of tensile and fatigue testing samples of LPBFed CP-Ti on a build plate. (b) EBSD IPF maps of the as-built (ASB), HIPped at 730◦C and HIPped at 950◦C showing grain coarsening after HIP treatments. (c) Yield strength of the LPBFed and wrought materials along various directions. (d) Effective fatigue threshold of LPBFed and wrought materials

Source: Hasib et al. 2021 [https://doi.org/10.1016/j.addma.2021.102027]

Commercially pure titanium

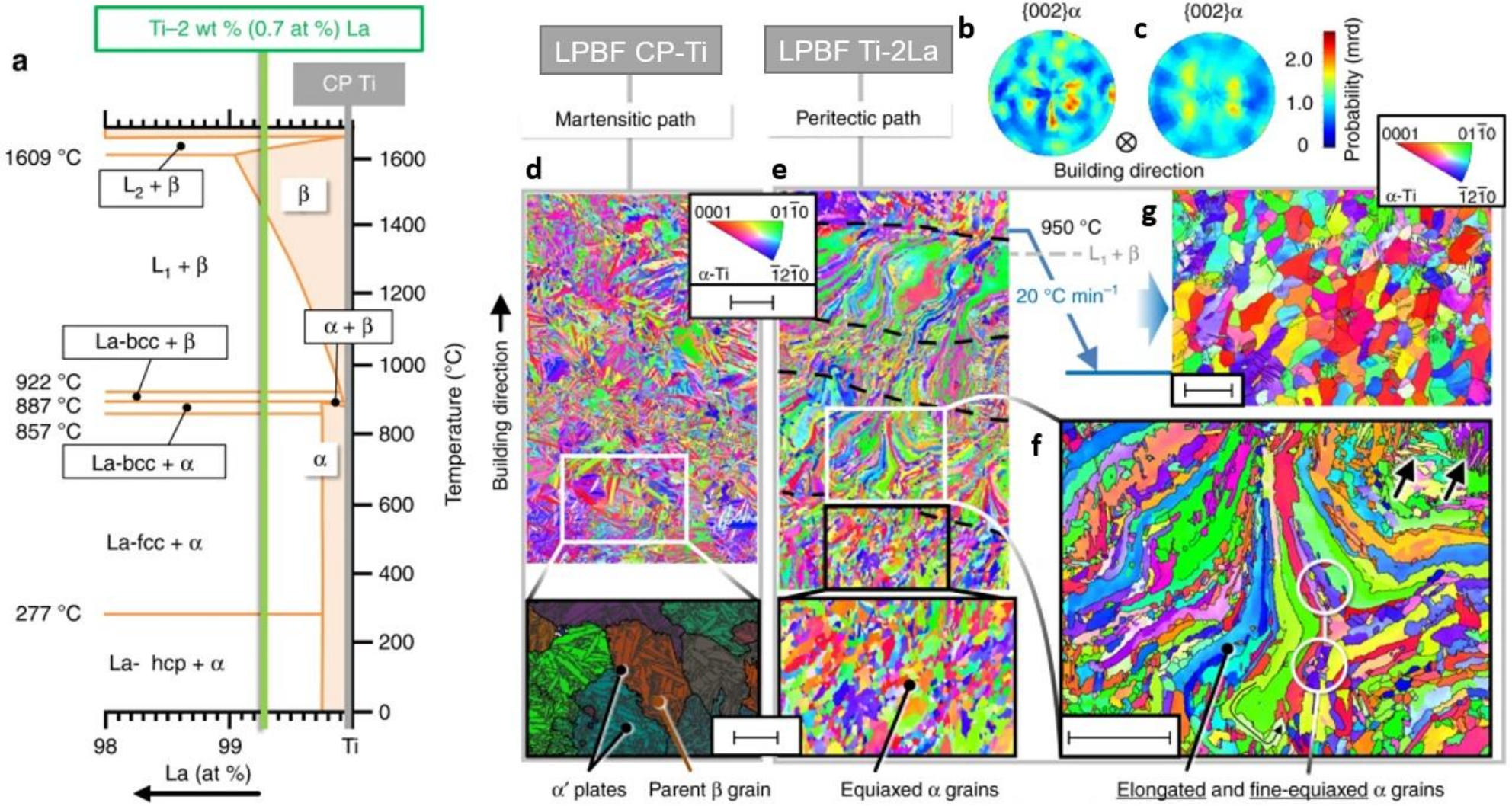

Fig. (a) Ti-La phase diagram showing the compositions used for LPBF, (b) and (c) Normalised pole figures of $\{002\}_{\alpha}$ for CP-Ti and Ti-2La, respectively, (d) EBSD IPF map showing orientation relationships of α'-martensite and parent β grains in LPBFed CP-Ti, (e) EBSD IPF map showing elongated and fine equiaxed α grains in LPBFed Ti-2La. (e) Post processing of the LPBFed Ti-2La with slow cooling from 950◦C passing through the peritectic line induces the formation of new grains and extensive lobularisation, resulting in a recrystallized-like microstructure. Scale bars of (d) and (e) are 100 µm, and scale bars of the magnified regions in (d) and (e), as well as (f) and (g) are 50 µm.

Source: Vila et al. 2018 [https://doi.org/10.1038/s41467-018-05819-9]

Commercially pure titanium

Fig. EBSD IPF map of an EBMed CP-Ti showing a weak texture, resulting in asotropic mechanical tensile properties

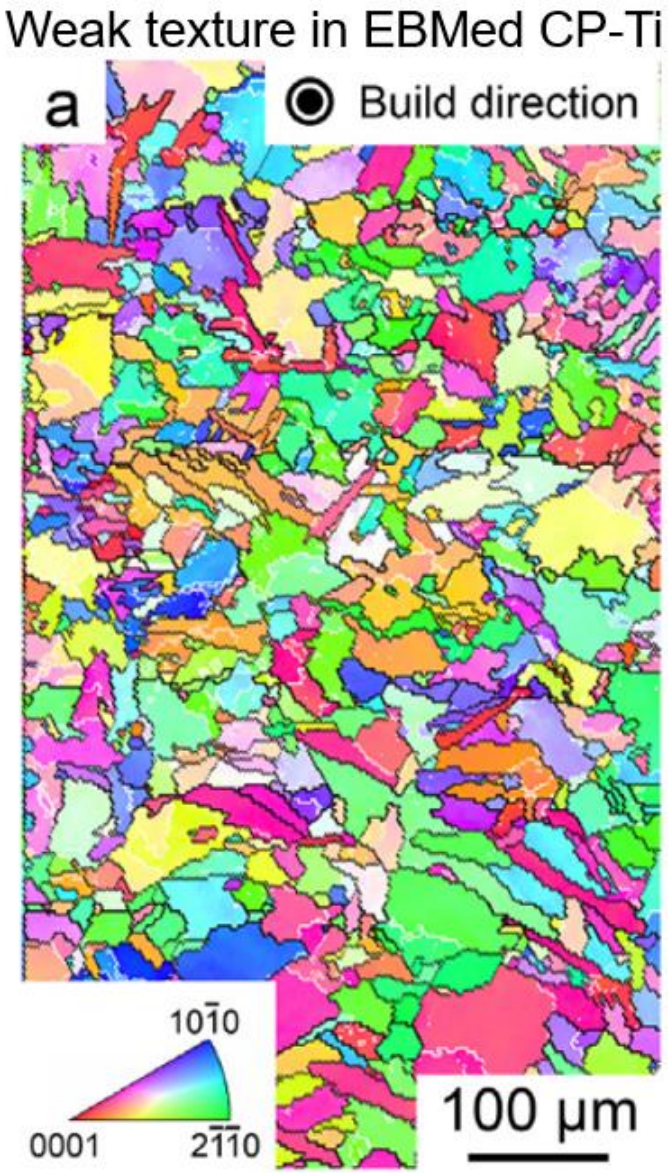

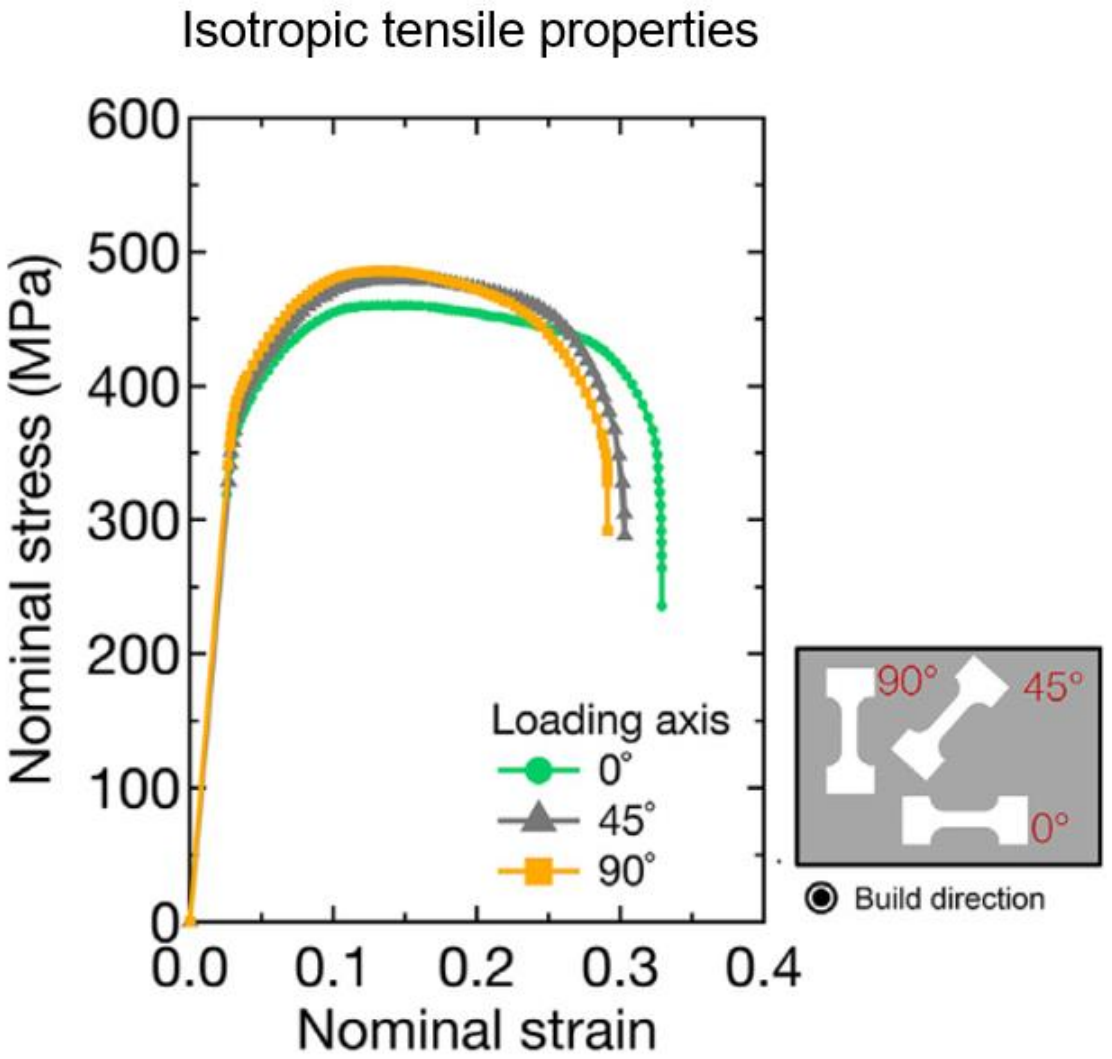

Source: Yamanaka et al. 2015 [https://doi.org/10.1016/j.addma.2015.09.007]

Commercially pure titanium

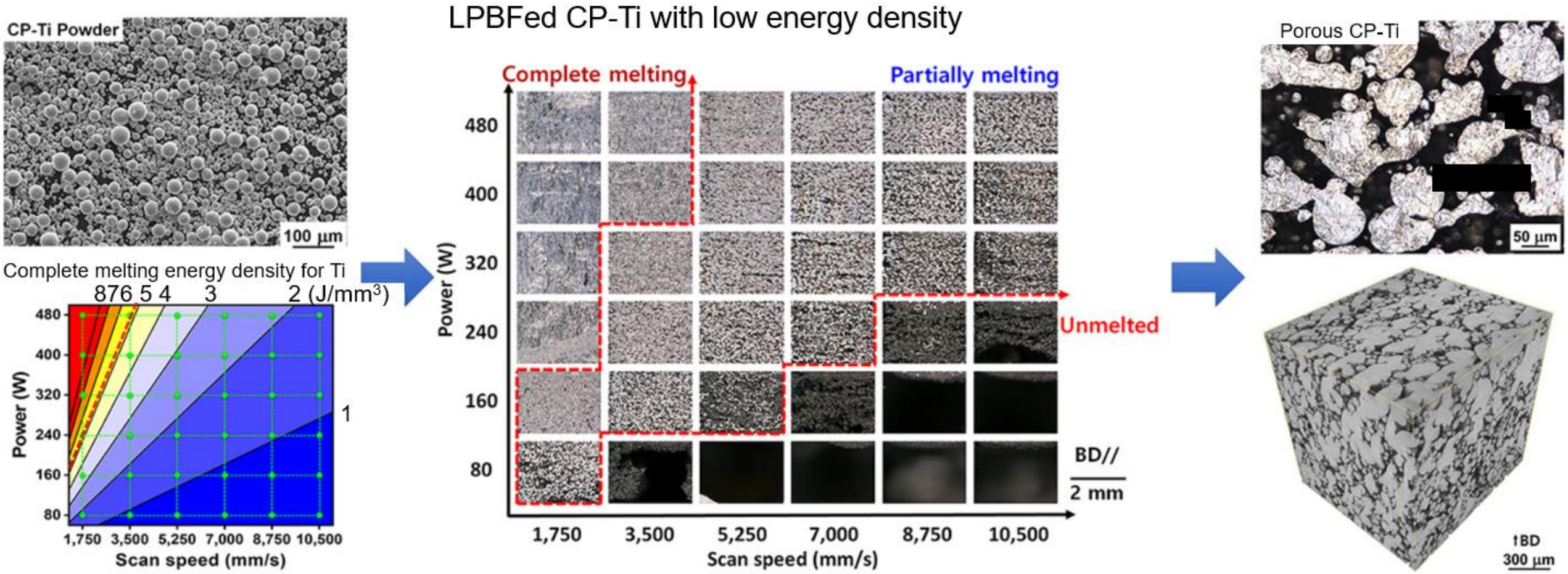

Fig. Fabrication of porous CP-Ti by LPBF with a wide range of processing parameters. The green dots in the diagram in bottom right denote the laser power and scan speed; the red dotted line indicates the required minimum energy density for the complete melting of Ti

Source: Kim et al. 2020 [https://doi.org/10.1016/j.matdes.2020.109035]

β titanium alloys

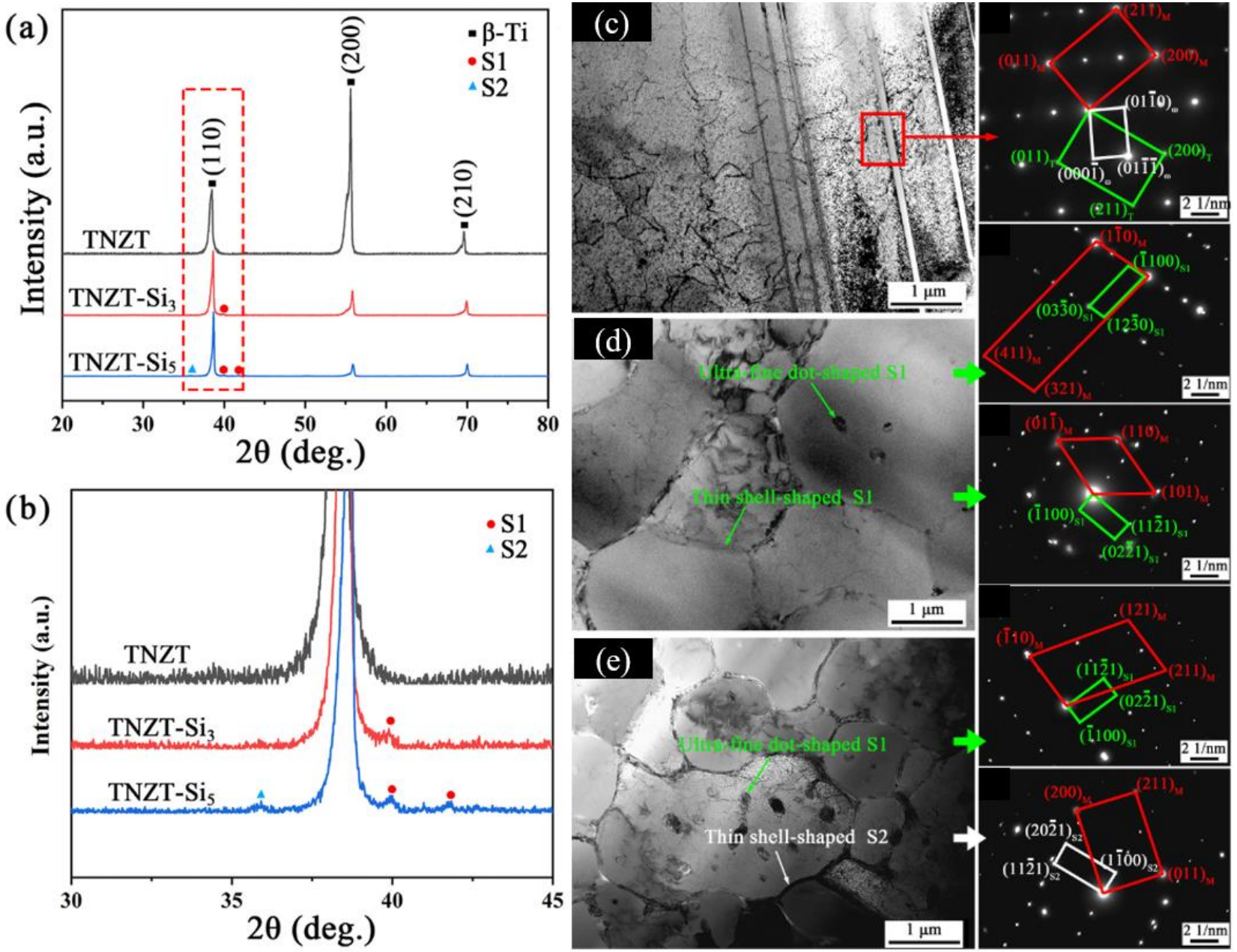

Fig. (a) XRD patterns of LPBFed TNZT-Si_x (x = 0, 3, 5 at.%) alloys and (b) magnified patterns for the area marked red in (a), (c) TEM micrographs of the LPBFed TNZT and the corresponding SAD patterns of twins (marked as red rectangles), (d) TEM micrograph of the LPBFed TNZT-Si_3 and the corresponding intragranular and intergranular SAD patterns of the S1 phase, and (e) TEM micrograph of the LPBFed TNZT-Si_5 and the corresponding SAD patterns of S1 and S2 phases

Source: Luo et al. 2022 [https://doi.org/10.1016/j.msec.2021.112625]

β titanium alloys

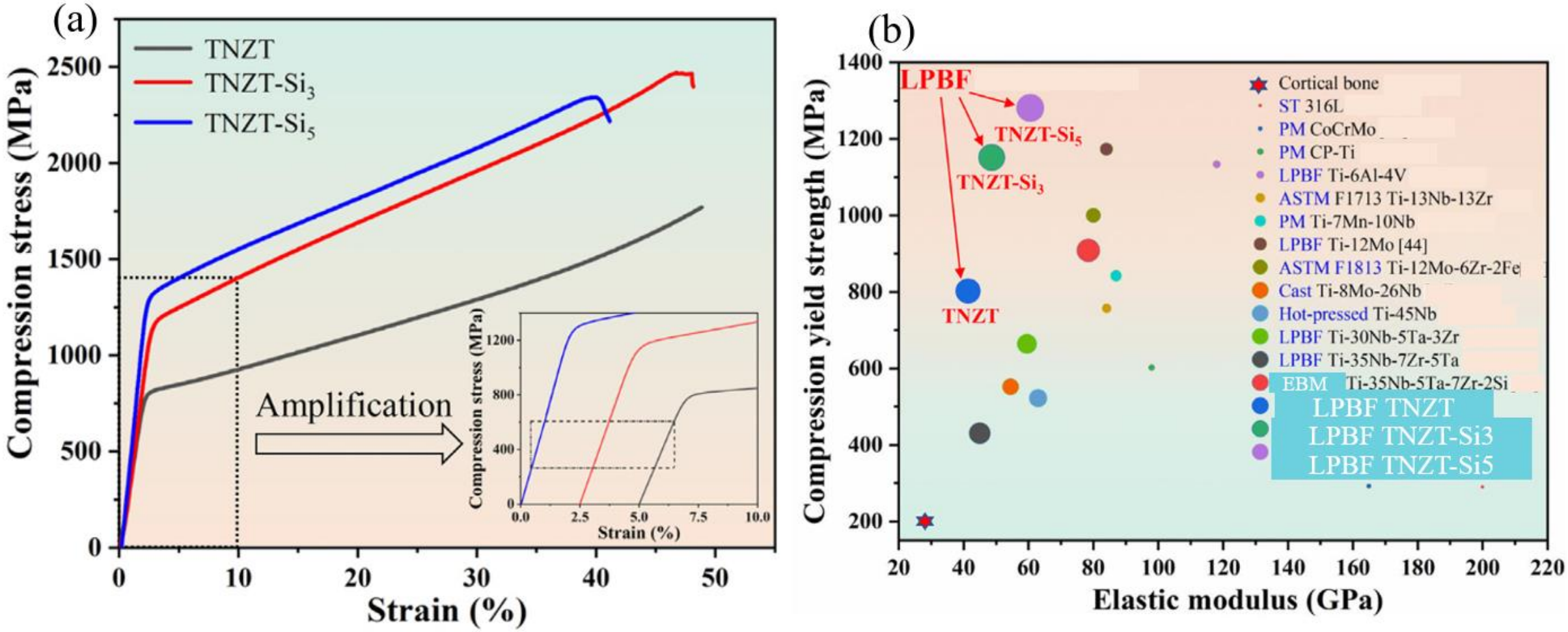

Fig. (a) Room temperature compressive stress-strain curves of the LPBFed TNZT-Six alloys, and (b) Compression yield strengths and elastic moduli of the LPBFed TNZT alloys and other previously reported biomedical alloys fabricated using solution treatment, powder metallurgy, casting, hot pressing, and EBM

Source: Luo et al. 2022 [https://doi.org/10.1016/j.msec.2021.112625]

β titanium alloys

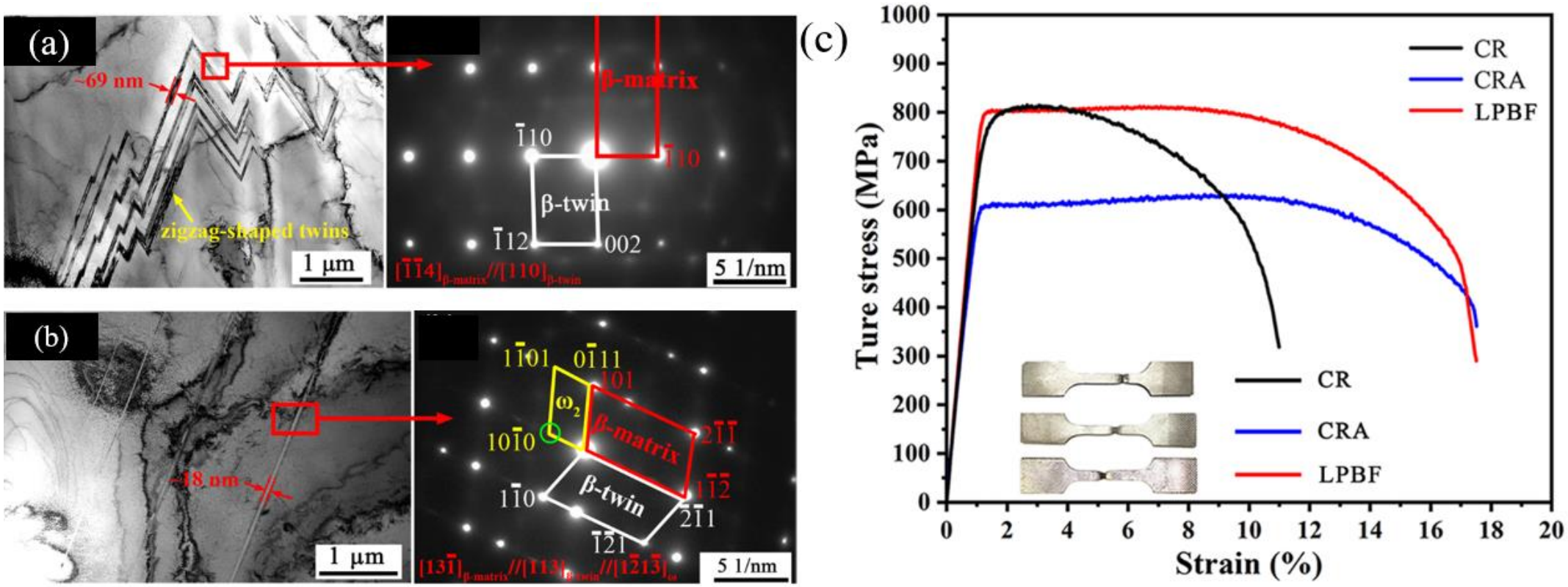

Fig. (a) TEM micrograph showing zigzag-shaped mechanical twins and the corresponding SAD pattern in the LPBFed as-built TNZT sample, (b) TEM micrograph showing lamellar mechanical twins and the corresponding SAD pattern in the LPBFed as-built TNZT sample, and (c) Room temperature true stress-true strain curves exhibiting mechanical properties of LPBFed, cold rolled (CR) and cold rolled and annealed (CRA) TNZT

Source: Luo et al. 2022 [https://doi.org/10.1016/j.addma.2022.102640]